Atmos. Chem. Phys. Discuss., 15, 26025–26065, 2015
www.atmos-chem-phys-discuss.net/15/26025/2015/
doi:10.5194/acpd-15-26025-2015

Atmospheric Chemistry and Physics Discussions

Towards understanding the variability in biospheric CO_2 fluxes: using FTIR spectrometry and a chemical transport model to investigate the sources and sinks of carbonyl sulfide and its link to CO_2

Y. Wang[1], N. M. Deutscher[1,2], M. Palm[1], T. Warneke[1], J. Notholt[1], I. Baker[3], J. Berry[4], P. Suntharalingam[5], N. Jones[2], E. Mahieu[6], B. Lejeune[6], J. E. Campbell[7], A. Wolf[8], and S. Kremser[9]

[1]Institute of Environmental Physics, University of Bremen, Bremen, Germany
[2]University of Wollongong, Wollongong, Australia
[3]Colorado State University, Fort Collins, CO, USA
[4]Carnegie Institute of Washington, Stanford, CA, USA
[5]University of East Anglia, Norwich, UK
[6]Institute of Astrophysics and Geophysics, University of Liège, Liège, Belgium

[7]University of California, Merced, CA, USA
[8]Princeton University, Princeton, NJ, USA
[9]Bodeker Scientific, Alexandra, New Zealand

Received: 3 July 2015 – Accepted: 4 September 2015 – Published: 25 September 2015

Correspondence to: Y. Wang (w_yuting@iup.physik.uni-bremen.de)

Published by Copernicus Publications on behalf of the European Geosciences Union.

ACPD
15, 26025–26065, 2015

Abstract

Understanding carbon dioxide (CO_2) biospheric processes is of great importance because the terrestrial exchange drives the seasonal and inter-annual variability of CO_2 in the atmosphere. Atmospheric inversions based on CO_2 concentration measurements alone can only determine net biosphere fluxes, but not differentiate between photosynthesis (uptake) and respiration (production). Carbonyl sulfide (OCS) could provide an important additional constraint: it is also taken up by plants during photosynthesis but not emitted during respiration, and therefore is a potential mean to differentiate between these processes. Solar absorption Fourier Transform InfraRed (FTIR) spectrometry allows for the retrievals of the atmospheric concentrations of both CO_2 and OCS from measured solar absorption spectra. Here, we investigate co-located and quasi-simultaneous FTIR measurements of OCS and CO_2 performed at three selected sites located in the Northern Hemisphere. These measurements are compared to simulations of OCS and CO_2 using a chemical transport model (GEOS-Chem). The OCS simulations are driven by different land biospheric fluxes to reproduce the seasonality of the measurements. Increasing the plant uptake of Kettle et al. (2002a) by a factor of three resulted in the best comparison with FTIR measurements. However, there are still discrepancies in the latitudinal distribution when comparing with HIPPO (HIAPER Pole-to-Pole Observations) data spanning both hemispheres. The coupled biospheric fluxes of OCS and CO_2 from the simple biosphere model (SiB) are used in the study and compared to measurements. The CO_2 simulation with SiB fluxes agrees with the measurements well, while the OCS simulation reproduced a weaker drawdown than FTIR measurements at selected sites, and a smaller latitudinal gradient in the Northern Hemisphere during growing season. An offset in the timing of the seasonal cycle minimum between SiB simulation and measurements is also seen. Using OCS as a photosynthesis proxy can help to understand how the biospheric processes are reproduced in models and to further understand the carbon cycle in the real world.

ACPD
15, 26025–26065, 2015

1 Introduction

Understanding the carbon dioxide (CO_2) biospheric processes within the carbon cycle is of great importance, because: (1) the land carbon sink absorbs more than a quarter of the CO_2 emissions released by human activities, which mitigates the increase of atmospheric CO_2 concentration, and (2) terrestrial exchange drives CO_2 variability in the atmosphere on seasonal and inter-annual time scales. The total biospheric CO_2 flux (net ecosystem production, NEP) is the sum of two much larger terms with different seasonality and drivers: the carbon uptake of gross primary production (GPP) and the release via respiration (Re). These fluxes are co-located, therefore, typically only information about their sum (the NEP) is available when they are quantified. To improve our knowledge of CO_2 biospheric processes, in particular how ecosystems will respond to a changing climate, we would ideally like to understand the individual contributions of these two fluxes.

Laboratory experiments (e.g. Goldan et al., 1988) have studied the pathway for carbonyl sulfide (OCS) uptake by plants, which is similar to the uptake mechanism of CO_2 during photosynthesis. Unlike CO_2, OCS uptake is a one-way process, and it is not emitted during respiration. Therefore OCS could be used to differentiate between photosynthesis and respiration fluxes of CO_2 (Campbell et al., 2008). Flask measurements of OCS in the Northern Hemisphere show a clear seasonal variation with a maximum in early spring and minimum in autumn, which is similar to the seasonality of CO_2 (Montzka et al., 2007) as biospheric fluxes are the main driver of the seasonal cycles for both species (Kettle et al., 2002a).

However, our knowledge about the sources and sinks of OCS remains limited. The estimates for the global budget still have significant uncertainties. This makes it difficult to use OCS as a photosynthetic tracer. The identified OCS sources include ocean emissions (direct emission and indirect emission via oxidation of carbon disulfide (CS_2) and dimethyl sulfide (DMS)), anthropogenic releases (direct emission and indirect emission via oxidation of CS_2), biomass burning, and volcanoes. The sinks are plant uptake, soil

ACPD
15, 26025–26065, 2015

uptake, reaction with hydroxyl radicals (OH), reaction with oxygen atoms (O), and photolysis in the stratosphere. The ocean is believed to be the most important source of OCS, and makes the biggest contribution to the seasonality of OCS in the Southern Hemisphere. Plant uptake is commonly recognized as the main sink of OCS, and is the dominant driver of seasonal variation in the Northern Hemisphere. Kettle et al. (2002a) analyzed OCS monthly fluxes, and then calculated the global annual sources and sinks, which are in balance within uncertainties. More recent studies (Suntharalingam et al., 2008; Berry et al., 2013) indicated that the plant uptake in Kettle's estimation is too small, and therefore a corresponding increase in sources is necessary to maintain the annual balance in the OCS budget. New studies have also shown that the ocean and anthropogenic source have been underestimated (Campbell et al., 2015; Launois et al., 2015) in Kettle et al. (2002a). Therefore, improving the estimation of the OCS sources and sinks is important when using it to investigate the biospheric fluxes of CO_2. To achieve this aim, more measurements are needed to validate the estimates.

Until now, the measurement data used for this OCS study are sparse. The typical measurements involved, such as the NOAA/ESRL/GMD network, include ground-based and aircraft flask sampling data. These ground-based in-situ measurements are only at limited sites and aircraft measurements cover relatively short time periods. The emerging of the remote sensing data (ground-based and satellite, Kuai et al., 2013) will potentially increase the number of OCS measurements largely. Ground-based solar absorption Fourier Transform InfraRed (FTIR) spectrometry measures the absorption of both CO_2 and OCS. They can be used to retrieve the total and/or partial atmospheric columns of these two gases. The FTIR OCS retrievals are sensitive at low altitude and can capture the variations due to the biospheric processes.

There are two networks of ground-based Fourier Transform InfraRed Spectrometers, both recording high resolution solar absorption spectra: the Total Carbon Column Observing Network (TCCON, http://www.tccon.caltech.edu; Wunch et al., 2011), concentrating on CO_2 and methane in the near-infrared (NIR); and the Network for the Detection of Atmospheric Composition Change InfraRed Working Group (NDACC-IRWG),

ACPD
15, 26025–26065, 2015

measuring spectra in the mid-infrared (MIR). CO_2 total columns are retrieved from NIR spectra, while OCS profiles and columns can be calculated from MIR spectra using dedicated software packages. CO_2 could also be retrieved from MIR spectra, but the retrieval sensitivity dominates in the stratosphere, and therefore the CO_2 seasonal cycle cannot be well captured (Barthlott et al., 2015; Buschmann et al., 2015). We will only use TCCON CO_2 product in this study. The NDACC-IRWG sites provide a potential database of OCS, that could be used to assess its sources and sinks. Kettle et al. (2002b) used FTIR OCS total column measurements to estimate hemisphere-integrated OCS flux and confirmed their understanding of OCS global budget. However, the measurements could not put constraints on the relative magnitude of vegetative uptake and ocean-related emissions. Lejeune et al. (2015) has improved the OCS retrieval, with a better accuracy on seasonal amplitude, which is important for studying the carbon cycle and resolving temporal variability of OCS fluxes. Additionally, some sites measure in both NIR and MIR spectral regions, and therefore provide co-located and quasi-simultaneous CO_2 and OCS measurements.

The aim of this work is to exploit ground-based FTIR measurements of OCS to evaluate its sources and sinks, and further to use OCS as a tracer of photosynthesis. This is the first time using total/partial column data from FTIR networks to study the relationship between OCS and CO_2. When interpreted by models, total column measurements are much less sensitive to assumptions on the boundary layer mixing, because every molecule in the atmospheric column is detected, independent of whether it is at the surface or in the upper troposphere. In order to obtain realistic fluxes by inverse models, assumptions must be made on the vertical mixing in the atmosphere, which is currently a large uncertainty in the transport of most models (Wunch et al., 2011; Yang et al., 2007; Keppel-Aleks et al., 2011). In our case this is quite important because the concentration profiles of CO_2 and OCS are different. Therefore, column measurements of OCS and CO_2 could provide additional information for evaluating their terrestrial exchange.

ACPD
15, 26025–26065, 2015

In Sects. 2–4, we will describe the measurements, models, and inter-comparison between FTIR and model, respectively. In Sects. 5, we first analyze the FTIR measurements of OCS and CO_2 at selected sites. Then we compare OCS measurements to model simulations to evaluate the sources and sinks of OCS. Finally, we will discuss what can be learnt about CO_2 biospheric fluxes from OCS. The publication closes with the conclusion.

2 Measurements

2.1 FTIR

Three measurement sites are used in this study as a starting point for the research aim of using OCS to differentiate between photosynthetic and respiration fluxes of CO_2 (see details in Table 1). Ny-Ålesund and Bremen, which are operated by the University of Bremen, measure both OCS and CO_2. The Jungfraujoch FTIR, operated by the University of Liège, only measures in the MIR spectral region, and therefore TCCON-type CO_2 data are not available.

OCS profiles and total columns were retrieved using the SFIT-4 algorithm, based on the optimal estimation technique (Rodgers, 2000). A mixed spectroscopy based on the HITRAN 2012 database was used in the retrievals. The a priori profile of OCS was provided by Geoff Toon over communication, and modified according to the average tropopause height above each site (constant in the troposphere, and decrease above tropopause). Four spectral micro-windows were used in the fitting (Lejeune et al., 2015), containing the OCS $\nu 3$ band P32, P28, P25, and P18 lines, respectively. Before fitting, spectra with a signal-to-noise ratio (SNR) of less than 100 were discarded. Post-fitting, retrievals with a root-mean-square (RMS) residual of greater than 0.5 % were excluded before subsequent analysis. The retrieval parameters are summarized in Table 2.

ACPD
15, 26025–26065, 2015

To minimize the influence of the variations in stratosphere, the tropospheric partial columns were calculated from the surface to 9.8 km, based on the structure of the averaging kernels. In total, approximately 2.5 degrees of freedom for signal (DOFS) for total columns were obtained for all three sites. The DOFS for 0 to 9.8 km is about 1. To make the values comparable to the in situ measurements, the tropospheric OCS column-averaged dry-air mole fractions (xOCS) were derived using Eq. (1):

$$x\mathrm{OCS} = \text{Tropospheric OCS partial column}/\text{Tropospheric dry-air partial column} \quad (1)$$

The uncertainties are calculated using contributions from measurement uncertainties (S_m), and forward model parameter uncertainties (S_f) based on Rodgers (2000). The total uncertainty in the tropospheric partial columns (S_{total_tropo}) was determined by adding these two components at each tropospheric layer (i) in quadrature:

$$S_{total\_tropo} = \left(\sum_1^n (S_m(i)^2 + S_f(i)^2)\right)^{1/2} \quad (2)$$

The average uncertainties in the tropospheric partial columns from 2005 to 2012 are 1.55, 1.52, and 1.20 % for Ny-Ålesund, Bremen, and Jungfraujoch, respectively.

The OCS retrievals from the FTIR spectra are not calibrated to account for biases due to the spectroscopy and other factors, therefore the means of the FTIR and in-situ measurements have an offset.

CO_2 total columns as well as O_2 total columns were retrieved from near-infrared spectra using GFIT, following the TCCON standard procedure (Wunch et al., 2011). The CO_2 column is retrieved from two bands centered at 6228 and 6348 cm^{-1}, while O_2 is retrieved from the electronic band centered at 7882 cm^{-1}. CO_2 column-averaged dry-air mole fractions (DMF) were calculated by the following equation:

$$x\mathrm{CO_2} = \mathrm{CO_2}/\mathrm{O_2} \times 0.2095 \quad (3)$$

ACPD
15, 26025–26065, 2015

2.2 HIPPO

The HIPPO (HIAPER Pole-to-Pole Observations) study of carbon cycle and greenhouse gases provides pole-to-pole measurements of meteorology, atmospheric chemistry, and aerosol content over the Pacific Ocean. HIPPO flew five month-long missions between January 2009 and September 2011 at different seasons. In this work, we use the NOAA flask sample data product of HIPPO (Wofsy et al., 2012), which provides additional information on the latitudinal distribution of the OCS and CO_2. The OCS data (referred to as HIPPO-OCS) used in the work were measured by the NOAA "Whole Air Sampler-Montzka Mass Spectrometer #2" (NWAS-M2), while CO_2 concentrations (referred to as HIPPO-CO_2) were measured by the NOAA "Whole Air Sampler-Measurement of Atmospheric Gases that Influence Climate Change" (NWAS-MAGICC).

3 Model simulations

3.1 GEOS-Chem and CO_2 simulation

The GEOS–Chem chemical transport model (version v9-01-03) is used in this study to simulate the concentrations of CO_2 and OCS in the global atmosphere. It is driven by assimilated meteorological observations from the Goddard Earth Observing System (GEOS) of the NASA Global Modeling Assimilation Office (GMAO) (Bey et al., 2001). The simulations were run using GEOS-5 meteorology from 2004 to 2012 on a horizontal grid resolution of 2° by 2.5° (latitude by longitude), with 47 vertical levels. Taking 2004 as one year spin-up, we analyze the results from 2005 to 2012 based on hourly model output.

The CO_2 simulation module in GEOS-Chem was developed by Suntharalingam et al. (2003, 2004), and updated by Nassar et al. (2010). The CO_2 fluxes used in GEOS-Chem version v9-01-03 include monthly fluxes of fossil fuel emissions from

ACPD
15, 26025–26065, 2015

the Carbon Dioxide Information Analysis Center (CDIAC) inventory; biomass burning from the Global Fire Emission Database (GFED3); ocean exchange from Takahashi et al. (2009); and annual biofuel fluxes from Yevich and Logan (2003). GEOS-Chem uses CO_2 biospheric fluxes calculated from the Carnegie–Ames–Stanford–Approach (CASA; Olsen and Randerson, 2004) model for the year 2000 as a standard input, so that the biospheric fluxes do not have inter-annual variability. The CASA biospheric fluxes are balanced to zero at every grid, and therefore another terrestrial flux, which is referred to as the residual annual terrestrial exchange, is added to the simulation (Baker et al., 2006). In this study, we substitute the CASA biospheric fluxes with those calculated by the Simple Biosphere model (SiB; detail in Sect. 3.3).

3.2 OCS simulation

The OCS module is developed from the version of Suntharalingam et al. (2008), and added to GEOS-Chem v9-01-03. It is largely based on the gridded flux inventories of Kettle et al. (2002a), hereafter referred to as K2002. The input fluxes from K2002 include ocean emissions, anthropogenic emissions, plant uptake, and soil uptake. The OCS biomass burning emission is calculated from CO emissions (from GFED3) using a scale factor from Nguyen et al. (1995). The tropospheric OH oxidation of OCS is calculated from OH monthly data (Park et al., 2004) and a temperature dependent rate (Atkinson et al., 1997). In addition, we included stratospheric loss (total loss from reaction with OH, O, and photolysis) in the OCS simulation to avoid the OCS accumulation above the troposphere. This stratospheric loss is computed using the altitude dependent loss rate from Chin and Davis (1995). The OCS simulation with K2002 provides a baseline for evaluating the sources and sinks of OCS.

3.3 The Simple Biosphere model (SiB)

To study the relationship between OCS and CO_2, we used the coupled fluxes from SiB. SiB was developed as a lower boundary for atmospheric models (Baker et al., 2013;

ACPD
15, 26025–26065, 2015

Sellers et al., 1986), and has been coupled to General Circulation Models (GCMs; Sato et al., 1989; Randall et al., 1996) as well as mesoscale models (Denning et al., 2003; Nicholls et al., 2004; Wang et al., 2007; Corbin et al., 2008). Berry et al. (2013) incorporated the calculation of OCS uptake through stomata and in ground into SiB3 based on the biochemical mechanism for uptake of OCS by leaves and soils. This version of SiB is called SiB3-COS, and provides coupled simulations of CO_2 and OCS biospheric fluxes, including OCS plant uptake, OCS soil uptake, GPP, and CO_2 respiration. For this research, SiB3 simulations were performed on a 1.25° by 1.0° (latitude by longitude) grid, with meteorology provided by the Modern-Era Retrospective analysis for Research and Applications (MERRA; Reinecker et al., 2011). Precipitation fields were scaled to match Global Precipitation Climatology Project (GPCP; Adler et al., 2003) amplitudes globally. Respiration is scaled in SiB3, following Denning et al. (1996), to match productivity on a long-term basis; individual years are not in exact balance. Phenology (LAI, fPAR) is determined prognostically following Stöckli et al. (2008, 2011). Global GPP for the years 2000–2012 averages 120 $GtC\,year^{-1}$, in reasonable agreement with flux tower-based estimates (Beer et al., 2010; Jung et al., 2011), although the spatiotemporal distribution of carbon uptake and efflux is uncertain.

In SiB, the OCS plant uptake is not scaled from GPP using a single factor, but estimated by mechanistic parameterization, consisting of several steps (Berry et al., 2013). OCS first diffuses from the boundary layer to the canopy, then from the canopy to the stomata, the stomata to the cells, and then is consumed in the cells. In the first step, the diffusion amount depends on the boundary layer concentration and diffusion conductance. The subsequent diffusion steps also depend on the conductance. The diffusion pathway of OCS is the same as that of CO_2, but with different conductance. The consumption of OCS in the cells is by the enzyme carbonic anhydrase (CA), which is co-located with the enzyme that consumes CO_2 – Rubisco. CA activity and mesophyll conductance are suggested to be proportional to the V_{max} of Rubisco by some studies (Berry et al., 2013; Badger and Price, 1994; Evans et al., 1994), and this relationship is used in SiB to simulate the OCS uptake.

ACPD
15, 26025–26065, 2015

Soil uptake of OCS is a function of the activity of CA, as well as the condition of the soil (Berry et al., 2013; Van Diest and Kesselmeier, 2008). Due to the lack of information on soil CA activity, the soil uptake is instead calculated as a function of heterotrophic respiration (Rh), because measurements show that the OCS soil uptake is proportional to Rh (Yi et al., 2007). In Berry et al. (2013), the entire soil column was considered when scaling OCS soil uptake to Rh. Subsequent model versions have modified this treatment to consider only the top 20 cm of soil. Additionally, $J(\theta)$ (Eq. (4), Berry et al., 2013) is no longer monotonically increasing from wet to dry soil, but rather follows a function (as Rh does in SiB) that peaks at an "optimum" soil wetness based on soil character (Raich et al., 1991). Soil OCS uptake in SiB has been reduced from approximately one-half to around one-quarter of the uptake rate of the canopy, which is more in line with observations (Whelan et al., 2013).

In this work, all the simulations were ran using GEOS-Chem transport model. Two OCS land fluxes were used, K2002 and SiB, in the OCS simulations, summarized in Table 3. In the analysis, the simulations with different fluxes will be referred to as the fluxes names, as shown in Table 3.

4 Comparison between FTIR retrievals and model

When comparing FTIR data with model simulations, the a priori and vertical sensitivity of the retrievals must be considered. We use the method described by Rodgers and Connor (2003). The hourly model vertical profiles were selected at the nearest grid point to the measurement sites and at measurement hours. The OCS profiles were smoothed by the FTIR a priori and averaging kernels of each measurement following the equation.

$$X_s = X_a + \mathbf{A}(X_m - X_a) \quad (4)$$

ACPD
15, 26025–26065, 2015

where X_s, X_a and X_m are smoothed, a priori and model vertical profile, respectively, and **A** is the averaging kernel matrix. The tropospheric *x*OCS was then calculated using Eq. (1).

For CO_2 column retrievals, Eq. (4) is modified (Wunch et al., 2010) to yield:

$$C_s = C_a + h^T \times a^T \times (X_m - X_a) \quad (5)$$

where C_s and C_a are smoothed and a priori CO_2 column-averaged DMF, *h* describes the vertical summation, a is the TCCON absorber-weighted column averaging kernel. TCCON averaging kernels are largely dependent on the solar zenith angle. Here we use the standard TCCON averaging kernel product, which provides the averaging kernels at five degree solar zenith angle intervals. The averaging kernels used here are interpolated to the solar zenith angle at the time the measurement was made.

5 Results

5.1 The relationship between OCS and CO_2 in FTIR measurements

Weekly mean calculated *x*CO_2 and *x*OCS are shown in Fig. 1. Both CO_2 and OCS show clear seasonal variation with a maximum in spring and a minimum in autumn. At Ny-Ålesund and Bremen, OCS reaches its minimum about one month later than CO_2. The drawdown of CO_2 results from the sum of the photosynthesis uptake and respiration emission. When respiration exceeds photosynthesis, CO_2 starts increasing, while OCS is still decreasing due to the contribution of photosynthesis.

The FTIR measurements show a relative seasonal amplitude of OCS of about six times that of CO_2, which is similar to the ratio derived from in-situ measurements (Montzka et al., 2007). The different magnitudes of the seasonal amplitudes are attributed to the absence of respiration, and to the leaf-scale relative uptake (LRU) rate of OCS to CO_2. Some experiments have shown that plants prefer OCS to CO_2, and obtained a LRU in the range of 1.3–5.5 for different species (Sandoval-Soto et al., 2005;

ACPD
15, 26025–26065, 2015

Seibt et al., 2010; Stimler et al., 2010). If the LRU rate is known, the seasonal cycle of GPP can be determined from the OCS seasonal cycle, and measurements of OCS can be used to quantify GPP.

The seasonal amplitudes of both CO_2 (approximately 3 %) and OCS (approximately 18 %) in Ny-Ålesund are bigger than those in Bremen (approximately 2 and 13 % for CO_2 and OCS, respectively) and Jungfraujoch (approximately 10 % for OCS). This is caused by the effect of the boreal forest combined with advective transport. The photosynthesis in the boreal forest is strong during the polar day, leading to the rapid drawdown of both CO_2 and OCS, which can be clearly seen in the measurements at the Arctic sites. For Jungfraujoch, the seasonal amplitude is smaller than that in Bremen, which partly results from its high altitude, so that the variation in the lower atmosphere is not captured. Eliminating altitudes below 3.5 km (the altitude of Jungfraujoch) from the calculation of *x*OCS at Ny-Ålesund and Bremen decreases their seasonal cycle amplitude by approximately 10 %.

5.2 OCS sources and sinks implied from FTIR measurements and model comparisons

5.2.1 Initial simulation of OCS

Prior to using the model relationship between OCS and CO_2, we assess the accuracy of the OCS fluxes, starting with fluxes of K2002, referred to as the initial simulation.

The simulations of OCS with K2002 are shown as orange plus signs in Fig. 2. The initial simulation (K2002) underestimates the seasonal amplitude, as reported by previous studies (Suntharalingam et al., 2008; Berry et al., 2013). Plant uptake is thought to be the dominant driver of seasonal variation in the Northern Hemisphere, so increasing the plant uptake should increase the seasonal amplitude. K2002 used a model based on Net Primary Production (NPP) to calculate the plant uptake of OCS, assuming the

ACPD
15, 26025–26065, 2015

relative uptake rates for OCS and CO_2 were the same (Kettle et al., 2002a). That is,

$$\text{OCS uptake} = \text{NPP} \times [\text{OCS}]/[CO_2] \quad (6)$$

where [OCS] and $[CO_2]$ are the atmospheric concentrations of OCS and CO_2, respectively. Considering that OCS is taken up by plants irreversibly, while CO_2 is also released through respiration, and plants favor OCS over CO_2, a model based on GPP has been suggested to replace the NPP-based model (Sandoval-Soto et al., 2005):

$$\text{OCS uptake} = \text{GPP} \times [\text{OCS}]/[CO_2] \times \text{LRU} \quad (7)$$

GPP is about two times as large as NPP, and the global averaged LRU is in the range of 1.3–3.1 (Seibt et al., 2010; Stimler et al., 2012; Berkelhammer et al., 2014), so that in the GPP-based model, the OCS plant uptake is increased by a factor of 2.6 to 6.2 from the NPP model. Therefore the plant uptake in K2002 needs to be increased to match the seasonal cycle of the measurements.

5.2.2 Simulations with rescaled K2002 fluxes

In order to improve the OCS simulation, we rescaled the OCS fluxes to find a better match to the measurements. This scaling, while not realistic, provides an idea of the sensitivity of the simulation to these processes. Following Suntharalingam et al. (2008) we modified the K2002 fluxes by increasing the plant uptake by factors of two (K2002×2, Fig. 2 blue asterisks) and three (K2002×3, Fig. 2 green stars). To balance the global budget, the ocean emissions were modified based on previous studies, which include increasing the ocean emissions in the tropical region, and decreasing the ocean emissions in the Southern Ocean (Suntharalingam et al., 2008). This will be further discussed in Sect. 5.2.3. The details of the rescaled OCS sources and sinks are shown in Table 3.

The simulations with rescaled fluxes increased the seasonal cycle amplitudes, and decreased the peak and mean values at the measurement sites. For the Northern

ACPD
15, 26025–26065, 2015

Hemisphere, the rescaled plant fluxes mainly increased during growing season, causing a larger OCS drawdown. Combined with a small increase in the uptake during Northern winter, this leads to a decrease in the mean values. To maintain the balance in the global budget of OCS, lower fluxes in the boreal region must be compensated by larger fluxes elsewhere, thereby changing the latitudinal distribution. The seasonal amplitude of the simulation with K2002×2 matches the measurements better than the original Kettle fluxes. K2002×3 further increases the seasonal cycle amplitude. There is no inter-annual variability in the fluxes, so these simulations cannot reproduce the yearly varying seasonal amplitudes, which makes it difficult to judge the comparison between K2002×2 and K2002×3 for each year. However, from the averaged seasonal cycles (Fig. 2, right panels), the simulations with K2002×3 match the measurements better than K2002×2.

5.2.3 HIPPO latitudinal distribution

To evaluate the latitudinal distribution of the rescaled fluxes, we compared the model simulations with HIPPO-OCS (Fig. 3). To facilitate this comparison, the model mean was adjusted (by adding an offset of 30 ppt) to match the mean of the HIPPO measurements. The latitudinal distribution of the simulation with K2002 poorly matches the HIPPO-OCS. The K2002 simulation results in OCS concentrations that are too low in the tropics and too high in the Southern Hemisphere compared to the measurements from all five campaigns. In late northern summer (HIPPO-5) and autumn (HIPPO-2), the model is higher than the measurements in the boreal region, because the modeled plant uptake is too weak. After rescaling the plant uptake and ocean emissions, the latitudinal distribution of the simulation shows better agreement with HIPPO-OCS. In the Southern Hemisphere, the K2002×3 simulation has a higher value than K2002×2, caused by the larger ocean emissions in the tropics. There are still mismatches, especially in the northern temperate region during HIPPO-2 and HIPPO-3, likely because sources in this region are too low in the model. Increasing the ocean emissions in the Northern Hemisphere by a factor of two (not shown) results in a simulated increase

ACPD
15, 26025–26065, 2015

in OCS in northern summer, at the time that ocean fluxes are greatest, while winter is hardly affected. Simply rescaling the fluxes based on the distribution (temporal and spatial) of K2002 is not sufficient to reproduce the latitudinal gradient of OCS: the seasonal cycles of the fluxes also need to be reconsidered. In this work, the ocean emissions were only modified at certain latitudes by a single regionally-specific factor. For all simulations except K2002, a value of 0.5 was applied for the Southern Ocean (30–90° S), while in the tropics (30° N–30° S), values of 3.2, 5.1, and 5.2 were used for K2002×2, K2002×3, and SiB, respectively, to balance the global budget. Other studies used atmospheric inversions (Berry et al., 2013; Kuai et al., 2015) or an ocean general circulation and biogeochemistry model (Launois et al., 2015) to access the ocean fluxes, and gain better distribution. The global amount and general latitudinal distribution are consistent with this study.

The latitudinal gradient in the boreal region is more sensitive to plant uptake. Increasing plant uptake gives a steeper latitude gradient towards the Arctic. The simulation with K2002×3 reproduced the strong gradient in summer and autumn, but the values are lower than the measurements – in agreement with the comparison with FTIR measurements. The mean values of the simulation with K2002×3 at the selected stations are lower than the FTIR measurements.

5.3 Combination of OCS and CO_2 with SiB biospheric fluxes

Although there are still uncertainties in the OCS sources and sinks, apart from plant uptake, their effect on the seasonal cycle in the northern high latitudes is small. Unlike previous simulations of CO_2 and OCS, we used the coupled land fluxes of OCS and CO_2 from SiB to simultaneously simulate OCS and CO_2 with their seasonal cycles connected via the same modeled processes. Through the comparison of both species to the measurements, we can evaluate the GPP and Re in the biosphere model.

ACPD
15, 26025–26065, 2015

5.3.1 OCS simulation with SiB land fluxes

The OCS simulation results with SiB fluxes are shown as magenta triangles in Fig. 2. The mean values at the three sites are higher than those with the original or rescaled K2002 fluxes, especially at Ny-Ålesund. The seasonal amplitudes at Ny-Ålesund and Bremen are similar to those simulated with K2002×2; and the seasonal amplitude at Jungfraujoch is between those of K2002×2 and K2002×3. From Table 3, we can see that the plant uptake of SiB is about three times of K2002, and the soil uptake is also bigger than K2002. With identical distributions of these fluxes, one would expect a similar drawdown during growing season in the Northern Hemisphere from SiB compared to K2002×3. That this is not consistently present at the selected sites indicates that the latitudinal distribution of the land fluxes between SiB and Kettle is different.

We compared the difference between SiB and the scaled K2002 plant uptake and soil uptake in July, shown in Fig. 4. For the plant uptake, SiB is much smaller than K2002×3 in the boreal forest region, causing a smaller drawdown, while it is stronger in the tropical region. Figure 5 (top) shows the monthly plant uptake of different fluxes summed globally, and in three latitude bands: 30 to 90° N (North); 30° S to 30° N (Equatorial); and 90 to 30° S (South). In the North region, the total amount and seasonal variation of the SiB plant uptake are similar to K2002×2. The plant uptake of K2002 in the North region accounts for 42 % of the global total uptake in a year, while for SiB plant uptake, it contributes only 24 %. In Equatorial region the uptake in SiB is much larger than that in K2002×3. In the South, the plant uptake of SiB shows stronger seasonal variation than K2002×3. Globally, the SiB plant uptake is most consistent with K2002×3, though with a smaller seasonality, resulting from the strong uptake in the tropics and Southern Hemisphere. The difference in soil uptake between SiB and K2002 in July shows a similar pattern to the difference in plant uptake: larger uptake in the tropics and smaller uptake in the remaining regions. This latitudinal distribution of SiB OCS land fluxes leads to a higher mean value and smaller seasonal amplitude in the northern high latitudes,

ACPD
15, 26025–26065, 2015

as seen from Ny-Ålesund. The seasonal amplitude is better represented by SiB at the mid latitude site of Jungfraujoch.

Besides the seasonal amplitude, there are phase differences at Bremen and Jungfraujoch between the simulations with SiB fluxes and measurements. Due to the gap during polar winter, these cannot be evaluated at Ny-Ålesund. The simulation with SiB shows higher values in the wintertime, which are also seen in the simulations with original and rescaled Kettle's flux. SiB, however, does not have a mechanism for OCS efflux, so the mean overestimation of OCS concentration in winter is by necessity a function of source location/magnitude and/or transport. The simulation with SiB fluxes reaches the minimum earlier than the measurements. If we discount transport errors, this indicates that there is OCS uptake (either from plants or soils) in the real world past the time when model uptake has ceased. The minimum offset is not seen in the simulations with K2002×2 and K2002×3, and the seasonal variations of plant uptake are similar in SiB and K2002×2 in the Northern Hemisphere (Fig. 5, top), so the early minimum in SiB may result from the smaller soil uptake in autumn compared to K2002, which is shown in Fig. 6 (bottom). As mentioned in Sect. 3.3, the soil uptake used in this work is smaller than that in Berry et al. (2013). This could mean that the actual soil uptake is stronger or continues longer. However, the temporal and spatial pattern of K2002 fluxes is with large uncertainties: the plant uptake is estimated from the NPP-base model; the soil uptake is calculated using an empirical algorithm with the parameterization determined for one arable soil type only, which is a likely source of error (Kettle et al., 2002a). Therefore, the early minimum in SiB cannot be attributed to soil uptake through the comparison to K2002. Further investigation is needed to understand the minimum shift.

The comparison between the SiB simulation and HIPPO-OCS measurements is shown in magenta lines in Fig. 3. The simulation with SiB fluxes results in a lower value in the Southern Hemisphere than the rescaled Kettle fluxes. This matches the HIPPO-OCS better, because SiB has a stronger plant uptake in the tropics and Southern Hemisphere. For the Northern Hemisphere, the low OCS concentrations in the low

ACPD
15, 26025–26065, 2015

and mid latitudes (HIPPO-2, HIPPO-3) are due to a combination of sources and/or transport, as are the simulations with Kettle's fluxes. SiB did not capture the strong latitudinal gradient during growing season (HIPPO-5), indicating the plant uptake of OCS in SiB in the boreal forest is too small, at least for the year (2011) in question.

5.3.2 Implications for CO_2 fluxes in SiB from OCS comparison

We hope to gain additional information on the CO_2 biospheric fluxes with the help of OCS. Since the CO_2 and OCS uptake by photosynthesis is coupled in SiB, one can calculate the GPP using the OCS uptake amount. This evaluation is complicated, however, because OCS and CO_2 go through the diffusion and consumption steps independently in SiB. The LRU is a diagnostic quantity that comes out of the simulations following explicit calculation of CO_2 and OCS fluxes. LRU varies by vegetation type, season, and time of day with uncertainties. However, these fluxes can still be evaluated by combining the comparison of OCS and CO_2 between simulations and measurements.

As discussed in Sect. 5.3.1, SiB underestimated the OCS drawdown at Ny-Ålesund, and poorly represented the latitudinal gradient in the Northern Hemisphere. This indicates that the photosynthetic production could be underestimated in northern high latitudes. We examine this further by comparing the CO_2 simulations with measurements.

The simulation of CO_2 with SiB fluxes represents the seasonal cycles at Ny-Ålesund and Bremen well (Fig. 6, left panels), unlike with the OCS comparison. From the mean seasonal cycles (Fig. 6, right panels) the minima in the CO_2 seasonal cycles are later in the simulation than measurements, indicating that the rebound of CO_2 after growing season is slower. We also compared the CO_2 latitudinal distribution between HIPPO-CO_2 and model simulations (Fig. 7). The difference in the Southern Hemisphere between the HIPPO-CO_2 and model is very small, so the main disagreement is in the northern high latitudes. In late autumn (HIPPO-2), SiB gives lower values than the HIPPO data in the boreal region. This supports the slower rebound in comparison to the FTIR measurements. In spring (HIPPO-3), the simulation is higher than the HIPPO

ACPD
15, 26025–26065, 2015

measurements in the Arctic. Previous studies showed that SiB3 performed well in the forest region of North America (Schwalm et al., 2010), while did a poor job in some Arctic tundra regions, caused by an over-sensitivity to very low temperature (Fisher et al., 2014). During the northern growing season, the SiB simulation resulted in a strong latitudinal gradient, which matches the HIPPO measurements well (HIPPO-5), illustrating that the net CO_2 fluxes have a reasonable latitudinal distribution, unlike with the OCS simulation.

The seasonal cycle of OCS is mainly influenced by the plant uptake, which is connected with GPP, while CO_2 seasonality results from the sum of both GPP and Re. Huntzinger et al. (2012) have shown that models can get similar NEP with gross fluxes (GPP and Re) that differ by a factor of two or more. If OCS plant uptake is used as a proxy for GPP, one can infer that the GPP estimated in SiB is low in the northern boreal region, which can not be seen in the CO_2 simulation driven by NEP. Assuming a reasonable LRU, this means the Re in SiB must also be low, so that the weak uptake is cancelled out in the net flux. However, the LRU is still uncertain. If LRU is low in general in the Northern Hemisphere, a reasonable GPP estimate could occur together with a small OCS uptake. Therefore the relationship of OCS and CO_2 in SiB needs to be further verified, but these results indicate that while the NEP is reasonably modeled, its individual component fluxes might be in error. This inference is made possible through the combination of OCS and CO_2 measurements.

The early minimum in SiB simulation compared to the measurements is indicative of weak uptake in the autumn. If this is caused by an early canopy shutdown, CO_2 assimilation would also stop early, leading to a shorter period of CO_2 drawdown in the simulation, which is the opposite of what is shown in Fig. 6. Therefore, it is more likely that soil uptake is too small in SiB in the autumn. Because the OCS soil uptake in SiB is proportional to Rh, the respiration could also be too small. This would explain the late minimum in the CO_2 simulation. Another possibility is that the LRU becomes very large in the autumn, so the OCS uptake is still strong while CO_2 uptake nearly stops. Experiments have shown that the LRU increases under low light condition (Stimler et al.,

ACPD
15, 26025–26065, 2015

2010). We do not have sufficient information at this time to determine the most likely reason for SiB to show a shift in the seasonal cycle minimum between the OCS simulation and the measurements. However, the combination of OCS and CO_2 atmospheric measurements opens some new avenues to explore how the biospheric models reproduce the carbon cycle in the real world.

6 Conclusions

For the first time, FTIR measurements of OCS and CO_2 were used to study their relationship. OCS retrieved from FTIR spectra at the three sites showed clear seasonal cycles, and confirmed the similarity to CO_2 variations.

We compared the OCS measurements to simulations with original and rescaled versions of fluxes based on Kettle et al. (2002a). The results indicate that increasing the plant uptake and ocean emissions improves the comparison. For the three selected sites in the Northern Hemisphere, increasing plant uptake by a factor of three represented the OCS seasonality well. The latitudinal distribution of the rescaled fluxes mismatches the HIPPO-OCS measurements in the northern temperate zone, implying a missing source in that region. Further studies are needed to optimize the OCS sources and sinks.

Simulations using coupled SiB land fluxes of CO_2 and OCS show good agreement of CO_2 with FTIR measurements at selected sites, but underestimated OCS drawdown. Through the comparison with HIPPO-OCS measurements, a weaker gradient in the Northern Hemisphere during growing season can be seen in the simulation. Using OCS as a GPP proxy, the GPP estimation in the Northern Hemisphere could be low in SiB. However, the relationship between OCS plant uptake and GPP in the model needs to be further verified.

The seasonal cycle minimum offset between simulation and measurements is not consistent for OCS and CO_2. The simulation presents an early minimum for OCS but a late minimum for CO_2 when compared to the measurements. These phase differ-

ACPD
15, 26025–26065, 2015

ences offer another aspect that can be used to evaluate the photosynthesis and respiration in SiB. Several possibilities which could cause this inconsistency have been discussed, but further research is needed before reaching a conclusion. Looking at OCS and CO_2 together inspires some new thoughts in how the biospheric models reproduce the carbon cycle in the real world.

7 Outlook

This work will be extended to more sites, including some in the Southern Hemisphere, to evaluate the seasonal cycles of OCS and CO_2 in different regions. The FTIR networks will provide an additional database for using OCS to constraint GPP, which would be further improved if more frequency, simultaneous measurements of OCS and CO_2 where available at a greater number of sites.

Using coupled OCS and CO_2 land fluxes in a biospheric model and comparing to measurements of both gases provides the method to constrain GPP with the help of OCS. The relationship between OCS and CO_2 uptake in SiB can be further verified by field measurements for more plant types and at different time. This will increase the confidence for making conclusions on GPP distribution and time variation from the view of OCS.

Although the relationship between OCS plant uptake and GPP still has uncertainties, OCS could be used to study the biospheric processes driving the inter-annual variability. Some climate extremes have impacts on both photosynthesis and respiration; for instance, high temperature could decrease photosynthetic production and increase respiration. With the help of OCS, these biospheric feedbacks could be distinguished.

Acknowledgements. This work is partly supported by the DFG, project PA 1714/6-1. Nicholas Deutscher is supported by an Australian Research Council – Discovery Early Career Researcher Award, DE140 100 178. We thank the AWI for support in carrying out the measurements in Ny-Ålesund, Spitsbergen. The University of Liège contribution to the present work has primarily been supported by the A3C and ACROSAT PRODEX projects (Belgian

ACPD
15, 26025–26065, 2015

Science Policy Office, BELSPO, Brussels). The Liege team further acknowledges crucial support by MeteoSwiss (GAW-CH), the F.R.S. – FNRS and the Fédération Wallonie-Bruxelles. We thank the International Foundation High Altitude Research Stations Jungfraujoch and Gornergrat (HFSJG, Bern). Additionally, we thank Steve Wofsy and all other HIPPO members for making the HIPPO and NOAA data available to the public from the HIPPO website at http://hippo.ornl.gov/.

The article processing charges for this open-access publication were covered by the University of Bremen.

References

Adler, A. F., Huffman, G. J., Chang, A., Ferraro, R., Xie, P.-P., Janowiak, J., Rudolf, B., Schneider, U., Curtis, S., Bolvin, D., Gruber, A., Susskind, J., Arkin, P., and Nelkin, E.: The Version-2 Global Precipitation Climatology Project (GPCP) monthly precipitation analysis (1979–present), J. Hydrometeorol., 4, 1147–1167, 2003.

Atkinson, R., Baulch, D. L., Cox, R. A., Hampson Jr., R. F., Kerr, J. A., Rossi, J. M., and Troe, J.: Evaluated kinetic, photochemical and heterogeneous data for atmospheric chemistry, J. Phys. Chem. Ref. Data, 26, 521–1011, 1997.

Badger, M. R. and Price, G. D.: The role of carbonic-anhydrase in photosynthesis, Annu. Rev. Plant Phys., 45, 369–392, 1994.

Baker, D. F., Law, R. M., Gurney, K. R., Rayner, P., Peylin, P., Denning, A. S., Bousquet, P., Bruhwiler, L., Chen, Y.-H., Ciais, P., Fung, I. Y., Heimann, M., John, J., Maki, T., Maksyutov, S., Masarie, K., Prather, M., Pak, B., Taguchi, S., and Zhu, Z.: TransCom 3 inversion intercomparison: impact of transport model errors on the interannual variability of regional CO_2 fluxes, 1988–2003, Global Biogeochem. Cy., 20, GB1002, doi:10.1029/2004GB002439, 2006.

Baker, I. T., Harper, A. B., da Rocha, H. R., Denning, A. S., Araújo, A. C., Borma, L. S., Freitas, H. C., Goulden, M. L., Manzi, A. O., Miller, S. D., Nobre, A. D., Restrepo-Coupe, N., Saleska, S. R., Stöckli, R., von Randow, C., and Wofsy, S. C.: Surface ecophysiological behavior across vegetation and moisture gradients in tropical South America, Agr. Forest Meteorol., 182, 177–188, doi:10.1016/j.agrformet.2012.11.015, 2013.

ACPD
15, 26025–26065, 2015

Barthlott, S., Schneider, M., Hase, F., Wiegele, A., Christner, E., González, Y., Blumenstock, T., Dohe, S., García, O. E., Sepúlveda, E., Strong, K., Mendonca, J., Weaver, D., Palm, M., Deutscher, N. M., Warneke, T., Notholt, J., Lejeune, B., Mahieu, E., Jones, N., Griffith, D. W. T., Velazco, V. A., Smale, D., Robinson, J., Kivi, R., Heikkinen, P., and Raffalski, U.: Using XCO_2 retrievals for assessing the long-term consistency of NDACC/FTIR data sets, Atmos. Meas. Tech., 8, 1555–1573, doi:10.5194/amt-8-1555-2015, 2015.

Beer, C., Reichstein, M., Tomelleri, E., Ciais, P., Jung, M., Carvalhais, N., Rödenbeck, C., Arain, M. A., Baldocchi, D., Bonan, G. B., Bondeau, A., Cescatti, A., Lasslop, G., Lindroth, A., Lomas, M., Luyssaert, S., Margolis, H., Oleson, K. W., Roupsard, O., Veenendaal, E., Viovy, N., Williams, C., Woodward, F. I., and Papale, D.: Terrestrial gross carbon dioxide uptake: global distribution and covariation with climate, Science, 329, 834–838, doi:10.1126/science.1184984, 2010.

Berkelhammer, M., Asaf, D., Still, C., Montzka, S., Noone, D., Gupta, M., Provencal, R., Chen, H., and Yakir, D.: Constraining surface carbon fluxes using in situ measurements of carbonyl sulfide and carbon dioxide, Global Biogeochem. Cy., 28, 161–179, doi:10.1002/2013GB004644, 2014.

Berry, J., Wolf, A., Campbell, J. E., Baker, I., Blake, N., Blake, D., Denning, A. S., Kawa, S. R., Montzka, S. A., Seibt, U., Stimler, K., Yakir, D., and Zhu, Z.: A coupled model of the global cycles of carbonyl sulfide and CO_2: a possible new window on the carbon cycle, J. Geophys. Res.-Biogeo., 118, 842–852, 2013.

Bey, I., Jacob, D. J., Yantosca, R. M., Logan, J. A., Field, B. D., Fiore, A. M., Li, Q., Liu, H. Y., Mickley, L. J., and Schultz, M. G.: Global modeling of tropospheric chemistry with assimilated meteorology: model description and evaluation, J. Geophys. Res.-Atmos., 106, 23073–23095, doi:10.1029/2001JD000807, 2001.

Buschmann, M., Deutscher, N. M., Sherlock, V., Palm, M., Warneke, T., and Notholt, J.: Retrieval of xCO_2 from ground-based mid-infrared (NDACC) solar absorption spectra and comparison to TCCON, Atmos. Meas. Tech. Discuss., in review, 2015.

Campbell, J. E., Carmichael, G. R., Chai, T., Mena-Carrasco, M., Tang, Y., Blake, D. R., Vay, S. A., Collatz, G. J., Baker, I., Berry, J. A., Montzka, S. A., Sweney, C., Schnoor, J. L., and Stanier, C. O.: Photosynthetic control of atmospheric carbonyl sulfide during the growing season, Science, 322, 1085–1088, 2008.

ACPD
15, 26025–26065, 2015

Campbell, J. E., Whelan, M. E., Seibt, U., Smith, S. J., Berry, J. A., and Hilton, T. W.: Atmospheric carbonyl sulfide sources from anthropogenic activity: implications for carbon cycle constraints, Geophys. Res. Lett., 42, 3004–3010, 2015.

Chin, M. and Davis, D. D.: A reanalysis of carbonyl sulfide as a source of stratospheric background sulfur aerosol, J. Geophys. Res., 100, 8993–9005, 1995.

Corbin, K. D., Denning, A. S., Lu, L., Wang, J.-W., and Baker, I. T.: Possible representation errors in inversions of satellite CO_2 retrievals, J. Geophys. Res., 113, doi:10.1029/2007JD008716, 2008.

Denning, A. S., Collatz, G. J., Zhang, C., Randall, D. A., Berry, J. A., Sellers, P. J., Colello, G. D., and Dazlich, D. A.: Simulation of terrestrial carbon metabolism and atmospheric CO_2 in a general circulation model, Part I: Surface carbon fluxes, Tellus B, 48, 521–542, 1996.

Denning, A. S., Nicholls, M., Prihodko, L., Baker, I., Vidale, P.-L., Davis, K., and Bakwin, P.: Simulated variations in atmospheric CO_2 over a Wisconsin forest using a coupled ecosystem–atmosphere model, Glob. Change Biol., 9, 1241–1250, 2003.

Evans, J. R., Caemmerer, S. V., Setchell, B. A., and Hudson, G. S.: The relationship between CO_2 transfer conductance and leaf anatomy in transgenic tobacco with a reduced content of Rubisco, Aust. J. Plant Physiol., 21, 475–495, 1994.

Fisher, J. B., Sikka, M., Oechel, W. C., Huntzinger, D. N., Melton, J. R., Koven, C. D., Ahlström, A., Arain, M. A., Baker, I., Chen, J. M., Ciais, P., Davidson, C., Dietze, M., El-Masri, B., Hayes, D., Huntingford, C., Jain, A. K., Levy, P. E., Lomas, M. R., Poulter, B., Price, D., Sahoo, A. K., Schaefer, K., Tian, H., Tomelleri, E., Verbeeck, H., Viovy, N., Wania, R., Zeng, N., and Miller, C. E.: Carbon cycle uncertainty in the Alaskan Arctic, Biogeosciences, 11, 4271–4288, doi:10.5194/bg-11-4271-2014, 2014.

Goldan, P. D., Fall, R., Kuster, W. C., and Fehsenfeld, F. C.: Uptake of cos by growing vegetation: a major tropospheric sink, J. Geophys. Res., 93, 14186–14192, 1988.

Huntzinger, D., Post, W., Michelak, A., Wei, Y., Jacobsen, A., West, T. O., Baker, I., Chen, J., Davis, K., Hayes, D., Hoffman, F., Jain, A., Liu, S., McGuire, D., Neilson, R., Poulter, B., Tian, H., Thornton, P., Tomelleri, E., Viovy, N., Xiao, J., Zeng, N., Zhao, M., and Cook, R.: North American Carbon Project (NACP) regional interim synthesis: terrestrial biospheric model intercomparison, Ecol. Model., 232, 144–157, doi:10.1016/j.ecolmodel.2012.02.004, 2012.

Jung, M., Reichstein, M., Margolis, H. A., Cescatti, A., Richardson, A. D., Arain, M. A., Arneth, A., Bernhofer, C., Bonal, D., Chen, J., Gianelle, D., Gobron, N., Kiely, G., Kutsch, W.,

ACPD
15, 26025–26065, 2015

Lasslop, G., Law, B. E., Lindroth, A., Merbold, L., Montagnani, L., Moors, E. J., Papale, D., Sottocornola, M., Vaccari, F., and Williams, C.: Global patterns of land–atmosphere fluxes of carbon dioxide, latent heat, and sensible heat derived from eddy covariance, satellite, and meteorological observations, J. Geophys. Res., 116, G00J07, doi:10.1029/2010JG001566, 2011.

Keppel-Aleks, G., Wennberg, P. O., and Schneider, T.: Sources of variations in total column carbon dioxide, Atmos. Chem. Phys., 11, 3581–3593, doi:10.5194/acp-11-3581-2011, 2011.

Kettle, A. J., Kuhn, U., von Hobe, M., Kesselmeier, J., and Andreae, M. O.: Global budget of atmospheric carbonyl sulfide: temporal and spatial variations of the dominant sources and sinks, J. Geophys. Res.-Atmos., 107, 4658, doi:10.1029/2002JD002187, 2002a.

Kettle, A. J., Kuhn, U., von Hobe, M., Kesselmeier, J., Liss, P. S., and Andreae, M. O.: Comparing forward and inverse models to estimate the seasonal variation of hemisphere-integrated fluxes of carbonyl sulfide, Atmos. Chem. Phys., 2, 343–361, doi:10.5194/acp-2-343-2002, 2002b.

Kuai, L., Worden, J., Kulawik, S. S., Montzka, S. A., and Liu, J.: Characterization of Aura TES carbonyl sulfide retrievals over ocean, Atmos. Meas. Tech., 7, 163–172, doi:10.5194/amt-7-163-2014, 2014.

Kuai, L., Worden, J. R., Campbell, J. E., Kulawik, S. S., Lee, M., Weidner, R. J., Li, K., Montzka, S. A., Moore, F. L., Berry, J. A., Baker, I., Denning, S., Bian, H., Bowman, K., Liu, J., and Yung, Y.: Estimate of carbonyl sulfide tropical oceanic surface fluxes using aura tropospheric emission spectrometer observations, J. Geosphys. Res.-Atmos., accepted, doi:10.1002/2015JD023493, 2015.

Launois, T., Belviso, S., Bopp, L., Fichot, C. G., and Peylin, P.: A new model for the global biogeochemical cycle of carbonyl sulfide – Part 1: Assessment of direct marine emissions with an oceanic general circulation and biogeochemistry model, Atmos. Chem. Phys., 15, 2295–2312, doi:10.5194/acp-15-2295-2015, 2015.

Lejeune, B., Mahieu, E., and Servais, C.: Optimized approach to retrieve information on the tropospheric and stratospheric carbonyl sulfide (OCS) vertical distributions above Jungfraujoch from high-resolution FTIR solar spectra, in preparation, 2015.

Montzka, S. A., Calvert, P., Hall, B. D., Elkins, J. W., Conway, T. J., Tans, P. P., and Sweeney, C.: On the global distribution, seasonality, and budget of atmospheric carbonyl sulfide (COS) and some similarities to CO_2, J. Geophys. Res.-Atmos., 112, D09302, doi:10.1029/2006JD007665, 2007.

ACPD
15, 26025–26065, 2015

Nassar, R., Jones, D. B. A., Suntharalingam, P., Chen, J. M., Andres, R. J., Wecht, K. J., Yantosca, R. M., Kulawik, S. S., Bowman, K. W., Worden, J. R., Machida, T., and Matsueda, H.: Modeling global atmospheric CO_2 with improved emission inventories and CO_2 production from the oxidation of other carbon species, Geosci. Model Dev., 3, 689–716, doi:10.5194/gmd-3-689-2010, 2010.

Nguyen, B. C., Mihalopoulos, N., Putaud, J. P., and Bonsang, B.: Carbonyl sulfide emissions from biomass burning in the tropics, J. Atmos. Chem., 22, 55–65, 1995.

Nicholls, M. E., Denning, A. S., Prihodko, L., Vidale, P.-L., Baker, I., Davis, K., and Bakwin, P.: A multiple-scale simulation of variations in atmospheric carbon dioxide using a coupled biosphere–atmosphere model, J. Geophys. Res., 109, D18, doi:10.1029/2003JD004482, 2004.

Olsen, S. C. and Randerson, J. T.: Differences between surface and column atmospheric CO_2 and implications for carbon cycle research, J. Geophys. Res., 109, D02301, doi:10.1029/2003JD003968, 2004.

Park, R. J., Jacob, D. J., Field, B. D., Yantosca, R. M., and Chin, M.: Natural and transboundary pollution influences on sulfate-nitrate-ammonium aerosols in the United States: implications for policy, J. Geophys. Res., 109, D15204, doi:10.1029/2003JD004473, 2004.

Raich, J. W., Rastetter, E. B., Melillo, J. M., Kicklighter, D. W., Steudler, P. A., Peterson, B. J., Grace, A. L., Moore III, B., and Vorosmarty, C. J.: Potential net primary productivity in South America: application of a global model, Ecol. Appl., 1, 399–429, 1991.

Randall, D. A., Dazlich, D. A., Zhang, C., Denning, A. S., Sellers, P. J., Tucker, C. J., Bounoua, L., Berry, J. A., Collatz, G. J., Field, C. B., Los, S. O., Justice, C. O., and Fung, I.: A revised land surface parameterization (SiB2) for GCMs, Part III: the greening of the Colorado State University General Circulation Model, J. Climate, 9, 738–763, 1996.

Rienecker, M. M., Suarez, M. J., Gelaro, R., Todling, R., Bacmeister, J., Liu, E., Bosilovich, M. G., Schubert, S. D., Takacs, L., Kim, G.-K., Bloom, S., Chen, J., Collins, D., Conaty, A., da Silva, A., Gu, W., Joiner, J., Koster, R. D., Lucchesi, R., Molod, A., Owens, T., Pawson, S., Pegion, P., Redder, C. R., Reichle, R., Robertson, F. R., Ruddick, A. G., Sienkiewicz, M., and Woollen, J.: MERRA: NASA's modern-era retrospective analysis for research and applications, J. Climate, 24, 3624–3648, 2011.

Rodgers, C. D.: Inverse Methods for Atmospheric Sounding: Theory and Practice, Series Atmospheric, Oceanic and Planetary Physics, vol. 2, World Scientific, Singapore, 238 pp., 2000.

ACPD
15, 26025–26065, 2015

Rodgers, C. D. and Connor, B. J.: Intercomparison of remote sounding instruments, J. Geophys. Res., 108, 4116, doi:10.1029/2002JD002299, 2003.

Sandoval-Soto, L., Stanimirov, M., von Hobe, M., Schmitt, V., Valdes, J., Wild, A., and Kesselmeier, J.: Global uptake of carbonyl sulfide (COS) by terrestrial vegetation: Estimates corrected by deposition velocities normalized to the uptake of carbon dioxide (CO_2), Biogeosciences, 2, 125–132, doi:10.5194/bg-2-125-2005, 2005.

Sato, N., Sellers, P. J., Randall, D. A., Schneider, E. K., Shukla, J., Kinter, J. L., Hou, Y.-T., and Albertazzi, E.: Effects of implementing the Simple Biosphere Model in a General Circulation Model, J. Atmos. Sci., 46, 2757–2782, 1989.

Schwalm, C. R., Williams, C. A., Schaefer, K., Anderson, R., Arain, M. A., Baker, I., Barr, A., Black, T. A., Chen, G. S., Chen, J. M., Ciais, P., Davis, K. J., Desai, A., Dietze, M., Dragoni, D., Fischer, M. L., Flanagan, L. B., Grant, R., Gu, L. H., Hollinger, D., Izaurralde, R. C., Kucharik, C., Lafleur, P., Law, B. E., Li, L. H., Li, Z. P., Liu, S. G., Lokupitiya, E., Luo, Y. Q., Ma, S. Y., Margolis, H., Matamala, R., McCaughey, H., Monson, R. K., Oechel, W. C., Peng, C. H., Poulter, B., Price, D. T., Riciutto, D. M., Riley, W., Sahoo, A. K., Sprintsin, M., Sun, J. F., Tian, H. Q., Tonitto, C., Verbeeck, H., and Verma, S. B.: A model-data intercomparison of CO_2 exchange across North America: results from the North American Carbon Program site synthesis, J. Geophys. Res.-Biogeo., 115, G00H05, doi:10.1029/2009JG001229, 2010.

Seibt, U., Kesselmeier, J., Sandoval-Soto, L., Kuhn, U., and Berry, J. A.: A kinetic analysis of leaf uptake of COS and its relation to transpiration, photosynthesis and carbon isotope fractionation, Biogeosciences, 7, 333–341, doi:10.5194/bg-7-333-2010, 2010.

Sellers, P. J., Mintz, Y., Sud, Y. C., and Dalcher, A.: A simple biosphere model (SIB) for use within general-circulation models, J. Atmos. Sci., 43, 505–531, 1986.

Stimler, K., Montzka, S. A., Berry, J. A., Rudich, Y., and Yakir, D.: Relationships between carbonyl sulfide (COS) and CO_2 during leaf gas exchange, New Phytol., 186, 869–878, 2010.

Stimler, K., Berry, J. A., and Yakir, D.: Effects of carbonyl sulfide and carbonic anhydrase on stomatal conductance, Plant Physiol., 158, 524–530, 2012.

Stöckli, R., Rutishauser, T., Dragoni, D., O'Keefe, J., Thornton, P. E., Jolly, M., Lu, L., and Denning, A. S.: Remote sensing data assimilation for a prognostic phenology model, J. Geophys. Res.-Biogeo., 113, G04021, doi:10.1029/2008JG000781, 2008.

ACPD
15, 26025–26065, 2015

Stöckli, R., Rutishauser, T., Baker, I., Körner, C., Liniger, M. A., and Denning, A. S.: A global reanalysis of vegetation phenology, J. Geophys. Res.-Biogeo., 116, G03020, doi:10.1029/2010JG001545, 2011.

Suntharalingam, P., Spivakovsky, C. M., Logan, J. A., and McElroy, M. B.: Estimating the distribution of terrestrial CO_2 sources and sinks from atmospheric measurements: sensitivity to configuration of the observation network, J. Geophys. Res., 108, 4452, doi:10.1029/2002JD002207, 2003.

Suntharalingam, P., Jacob, D. J., Palmer, P. I., Logan, J. A., Yantosca, R. M., Xiao, Y., Evans, M. J., Streets, D. G., Vay, S. L., and Sachse, G. W.: Improved quantification of Chinese carbon fluxes using CO_2/CO correlations in Asian outflow, J. Geophys. Res., 109, D18S18, doi:10.1029/2003JD004362, 2004.

Suntharalingam, P., Kettle, A. J., Montzka, S. M., and Jacob, D. J.: Global 3-D model analysis of the seasonal cycle of atmospheric carbonyl sulfide: implications for terrestrial vegetation uptake, Geophys. Res. Lett., 35, L19801, doi:10.1029/2008GL034332, 2008.

Takahashi, T., Sutherland, S. C., Wanninkhof, R., Sweeney, C., Feely, R. A., Chipman, D. W., Hales, B., Friederich, G., Chavez, F., Sabine, C., Watson, A., Bakker, D. C. E., Schuster, U., Metzl, N., Yoshikawa-Inoue, H., Ishii, M., Midorikawa, T., Nojiri, Y., Körtzinger, A., Steinhoff, T., Hoppema, M., Olafsson, J., Arnarson, T. S., Tilbrook, B., Johannessen, T., Olsen, A., Bellerby, R., Wong, C. S., Delille, B., Bates, N. R., and de Baar, H. J. W.: Climatological mean and decadal change in surface ocean pCO_2, and net sea–air CO_2 flux over the global oceans, Deep-Sea Res. Pt. II, 56, 554–577, doi:10.1016/j.dsr2.2008.12.009, 2009.

Van Diest, H. and Kesselmeier, J.: Soil atmosphere exchange of carbonyl sulfide (COS) regulated by diffusivity depending on water-filled pore space, Biogeosciences, 5, 475–483, doi:10.5194/bg-5-475-2008, 2008.

Wang, J. W., Denning, A. S., Lu, L., Baker, I. T., Corbin, K. D., and Davis, K. J.: Observations and simulations of synoptic, regional, and local variations in atmospheric CO_2, J. Geophys. Res., 112, D0418, doi:10.1029/2006JD007410, 2007.

Whelan, M. E., Min, D. H., and Rhew, R. C.: Salt marsh vegetation as a carbonyl sulfide (COS) source to the atmosphere, Atmos. Environ., 73, 131–137, 2013.

Wofsy, S. C., Daube, B. C., Jimenez, R., Kort, E., Pittman, J. V., Park, S., Commane, R., Xiang, B., Santoni, G., Jacob, D., Fisher, J., Pickett-Heaps, C., Wang, H., Wecht, K., Wang, Q.-Q., Stephens, B. B., Shertz, S., Watt, A. S., Romashkin, P., Campos, T., Haggerty, J., Cooper, W. A., Rogers, D., Beaton, S., Hendershot, R., Elkins, J. W., Fahey, D. W., Gao, R. S.,

ACPD
15, 26025–26065, 2015

Moore, F., Montzka, S. A., Schwarz, J. P., Perring, A. E., Hurst, D., Miller, B. R., Sweeney, C., Oltmans, S., Nance, D., Hintsa, E., Dutton, G., Watts, L. A., Spackman, J. R., Rosenlof, K. H., Ray, E. A., Hall, B., Zondlo, M. A., Diao, M., Keeling, R., Bent, J., Atlas, E. L., Lueb, R., and Mahoney, M. J.: HIPPO NOAA Flask Sample GHG, Halocarbon, and Hydrocarbon Data (R_20121129), Carbon Dioxide Information Analysis Center, Oak Ridge National Laboratory, Oak Ridge, Tennessee, USA, doi:10.3334/CDIAC/hippo_013 (release 29 November 2012), 2012.

Wunch, D., Toon, G. C., Wennberg, P. O., Wofsy, S. C., Stephens, B. B., Fischer, M. L., Uchino, O., Abshire, J. B., Bernath, P., Biraud, S. C., Blavier, J.-F. L., Boone, C., Bowman, K. P., Browell, E. V., Campos, T., Connor, B. J., Daube, B. C., Deutscher, N. M., Diao, M., Elkins, J. W., Gerbig, C., Gottlieb, E., Griffith, D. W. T., Hurst, D. F., Jiménez, R., Keppel-Aleks, G., Kort, E. A., Macatangay, R., Machida, T., Matsueda, H., Moore, F., Morino, I., Park, S., Robinson, J., Roehl, C. M., Sawa, Y., Sherlock, V., Sweeney, C., Tanaka, T., and Zondlo, M. A.: Calibration of the Total Carbon Column Observing Network using aircraft profile data, Atmos. Meas. Tech., 3, 1351–1362, doi:10.5194/amt-3-1351-2010, 2010.

Wunch, D., Toon, G. C., Blavier, J.-F. L., Washenfelder, R. A., Notholt, J., Connor, B. J., Griffith, D. W. T., Sherlock, V., and Wennberg, P. O.: The Total Carbon Column Observing Network, Philos. T. R. Soc. A, 369, 2087–2112, doi:10.1098/rsta.2010.0240, 2011.

Yang, Z., Washenfelder, R. A., Keppel-Aleks, G., Krakauer, N. Y., Randerson, J. T., Tans, P. P., Sweeney, C., and Wennberg, P. O.: New constraints on Northern Hemisphere growing season net flux, Geophys. Res. Lett., 34, L12807, doi:10.1029/2007GL029742, 2007.

Yevich, R. and Logan, J. A.: An assessment of biofuel use and burning of agricultural waste in the developing world, Global Biogeochem. Cy., 17, 1095, doi:10.1029/2002GB001952, 2003.

Yi, Z. G., Wang, X. M., Sheng, G. Y., Zhang, D. Q., Zhou, G. Y., and Fu, J. M.: Soil uptake of carbonyl sulfide in subtropical forests with different successional stages in south China, J. Geophys. Res., 112, D08302, doi:10.1029/2006JD008048, 2007.

ACPD
15, 26025–26065, 2015

Table 1. FTIR sites used in this study.

Site	Latitude (° N)	Longitude (° E)	Altitude (m a.s.l.)	Instrument	Measurement years	Network
Ny-Ålesund	78.9	11.9	21	120HR 120-5HR	1992–2012 2013–present	NDACC and TCCON
Bremen	53.1	8.8	27	120HR 125HR	2002–2003 2004–present	NDACC and TCCON
Jungfraujoch	46.5	8.0	3580	homemade 120HR	1984–2008 1990–present	NDACC

ACPD
15, 26025–26065, 2015

Table 2. Summary of the retrieval parameters for OCS.

Retrieval code	Spectroscopy	A priori OCS profiles	A priori S_a matrix	Microwindows (cm^{-1})	Interfering species	SNR	Pressure, Temperature profiles
SFIT4_v0.9.4	Based on HITRAN 2012	Provided by Geoff Toon over communication, modified by tropopause height	In-situ measurements variability below 9 km, ACE-FTS measurements variability above 9 km	2047.78–2048.22 2049.75–2050.12 2051.18–2051.48 2054.33–2054.67	O_3, H_2O, CO, $H_2^{18}O$, $^{13}CO_2$, ^{18}OCO	300 (pre-fixed)	NCEP

ACPD
15, 26025–26065, 2015

Table 3. Annual global atmospheric OCS budget (fluxes in Gg S year^{-1}).

	K2002[a] Mean (Range)	K2002×2 Revisions	K2002×3 Revisions	SiB Revisions
Sources				
Anthropogenic	182 (90–266)			
Ocean	280 (39–520)	516	754	757
Biomass burning	35 (25–38)[b]			
Sinks				
Plant	238 (210–270)	475	713	688
Soil	130 (74–180)			159
Tropospheric OH oxidation	96 (95–98)[b]			
Stratosphere loss	28[b]			
Net	5	4	4	3

[a] Modifications include biomass burning, tropospheric OH oxidation, and stratospheric loss (see text).
[b] The range for biomass burning and tropospheric OH oxidation is the range calculated in the model from 2005 to 2012; the calculated stratospheric loss varies little.

ACPD
15, 26025–26065, 2015

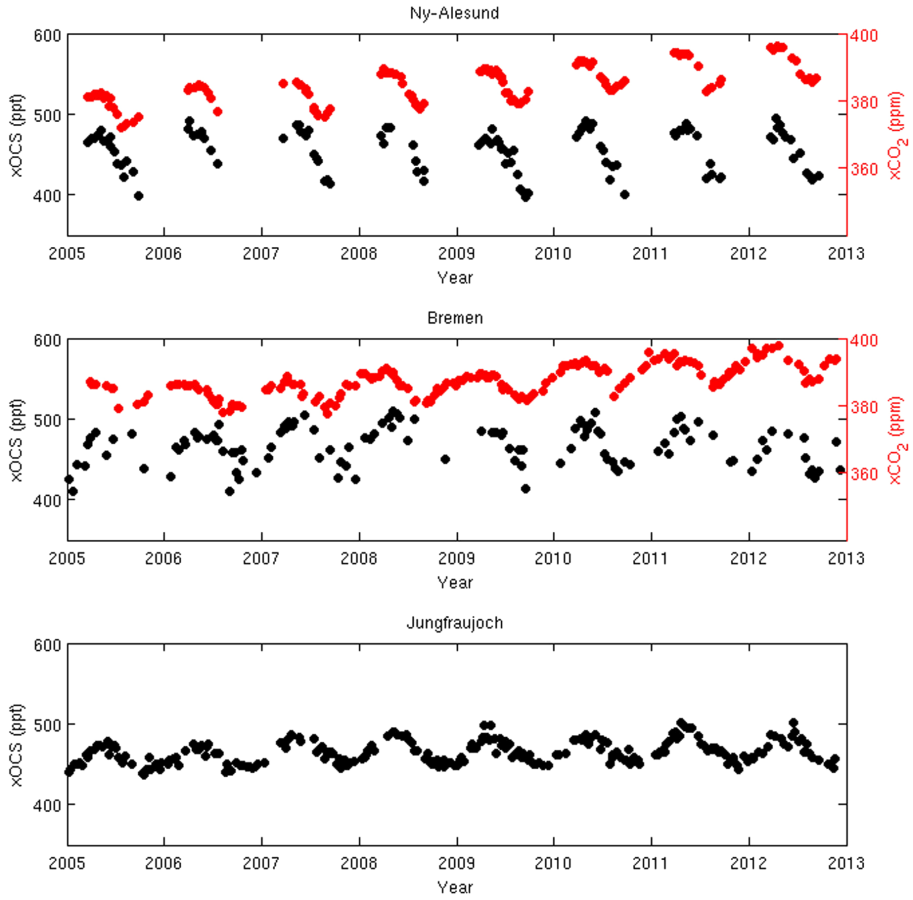

Figure 1. Weekly mean *x*OCS (black dots) and xCO_2 (red dots) retrieved from FTIR spectra at Ny-Ålesund (top), Bremen (middle) and Jungfraujoch (bottom).

ACPD
15, 26025–26065, 2015

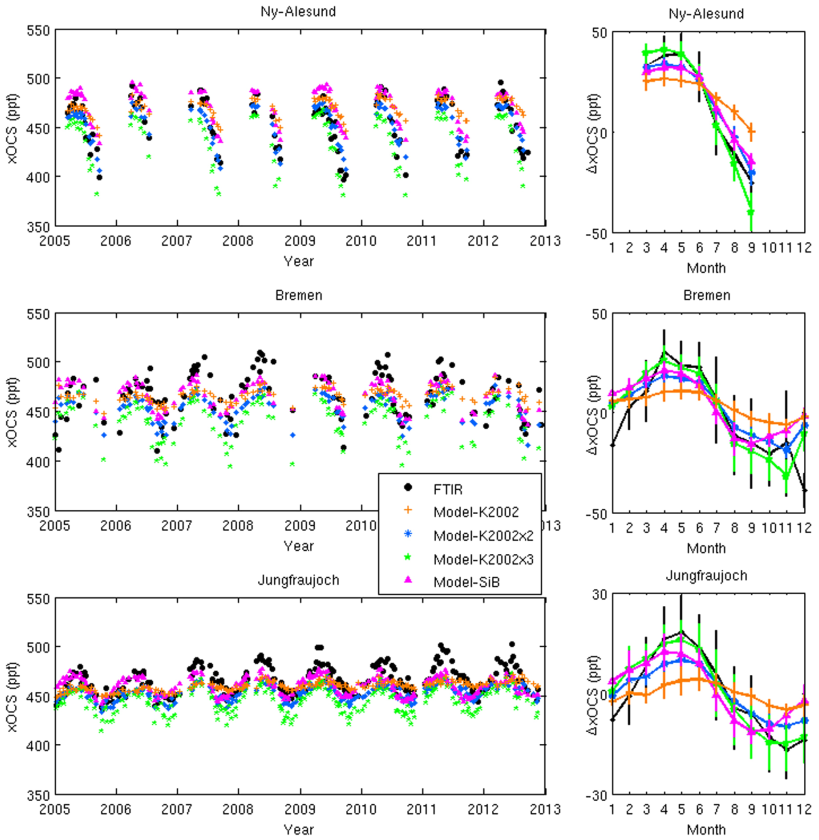

Figure 2. Comparison of FTIR measurements of OCS to model simulations at Ny-Ålesund (top), Bremen (middle) and Jungfraujoch (bottom). The left panels show weekly means from 2005 to 2012. The right panels are the monthly mean relative *x*OCS (relative to annual mean) averaged for multiple years. The error bars are the standard deviations of each month. The FTIR retrievals are shown in black dots. The model simulations are driven by K2002 (orange plus signs), K2002×2 (blue asterisks), K2002×3 (green stars), and SiB (magenta triangles).

ACPD
15, 26025–26065, 2015

Towards understanding the variability in biospheric CO_2 fluxes

Y. Wang et al.

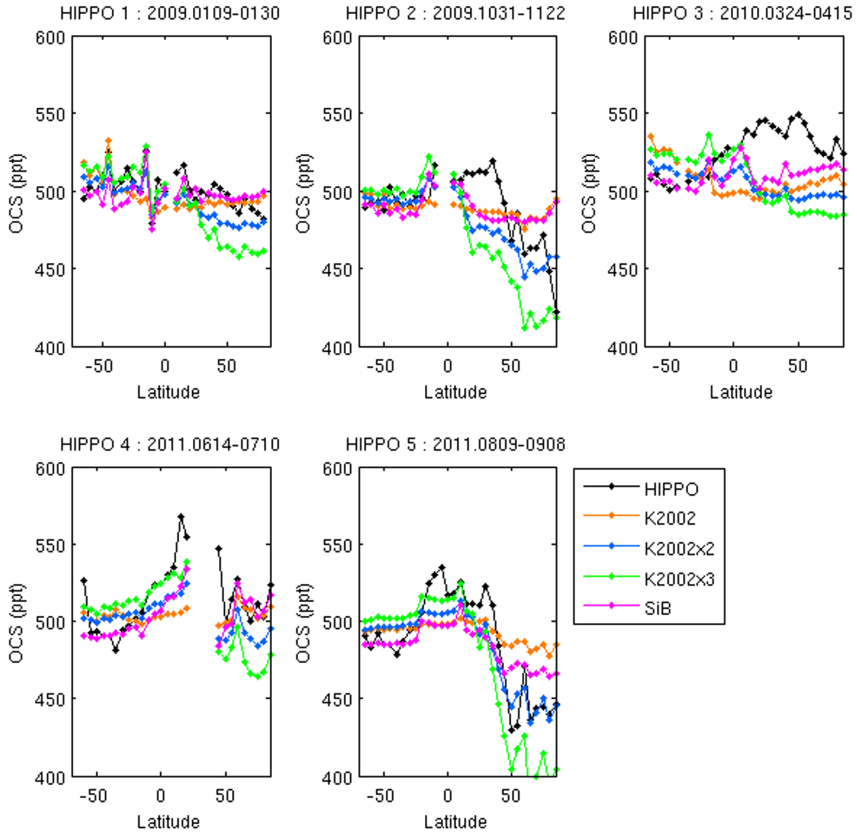

Figure 3. Comparison of HIPPO OCS measurements and model simulations. The five campaigns are compared separately to show latitudinal gradient at different seasons. To minimize the influence of the stratosphere, only the measurements lower than 9 km are used. The model outputs are selected at the nearest measurement location and time. The measurements and model output are averaged in five degree bins. The HIPPO data are shown in black dots. The model simulations are in the same colors with those shown in Fig. 2.

ACPD
15, 26025–26065, 2015

Towards understanding the variability in biospheric CO_2 fluxes

Y. Wang et al.

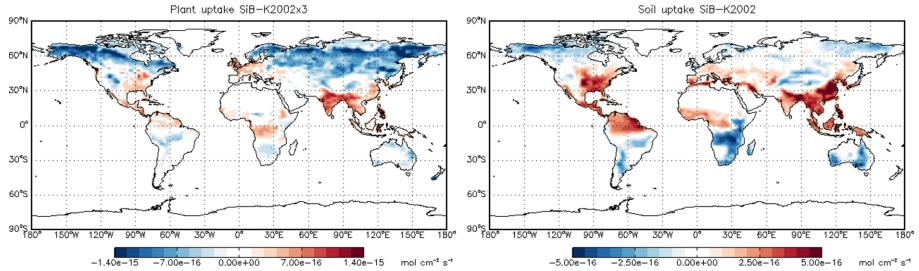

Figure 4. Difference between SiB OCS plant uptake and K2002×3 (left, SiB – K2002×3), difference between OCS soil uptake and K2002 (right, SiB – K2002).

ACPD
15, 26025–26065, 2015

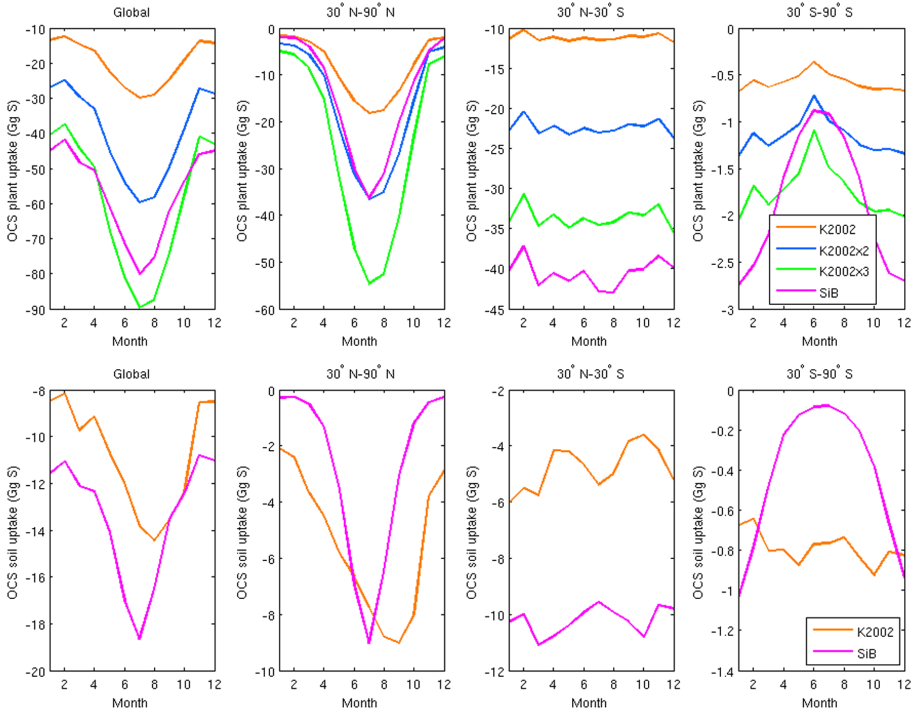

Figure 5. Monthly totals of OCS plant uptake (top) and soil uptake (bottom) of K2002 (orange), K2002×2 (blue), K2002×3 (green), and SiB (magenta) for global, 30–90° N, 30° N–30° S, and 30–90° S.

ACPD
15, 26025–26065, 2015

Towards understanding the variability in biospheric CO_2 fluxes

Y. Wang et al.

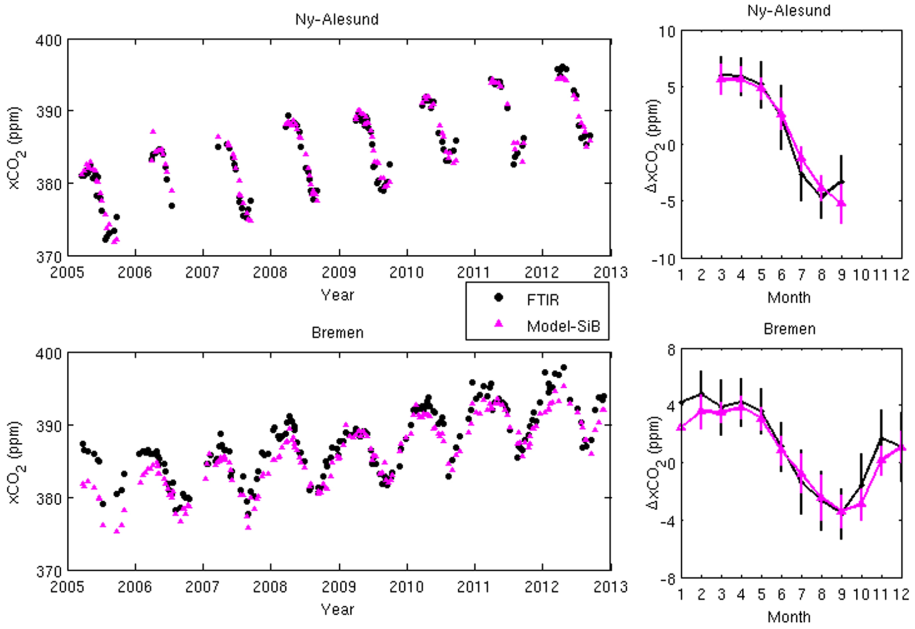

Figure 6. Comparison of FTIR measurements of CO_2 (black dots) to model simulations with SiB land fluxes (magenta triangles) at Ny-Ålesund (top) and Bremen (bottom). The left panels show weekly means from 2005 to 2012. The right panels show the monthly mean relative xCO_2 (relative to annual mean) averaged for multiple years. The error bars are the standard deviations of each month.

ACPD
15, 26025–26065, 2015

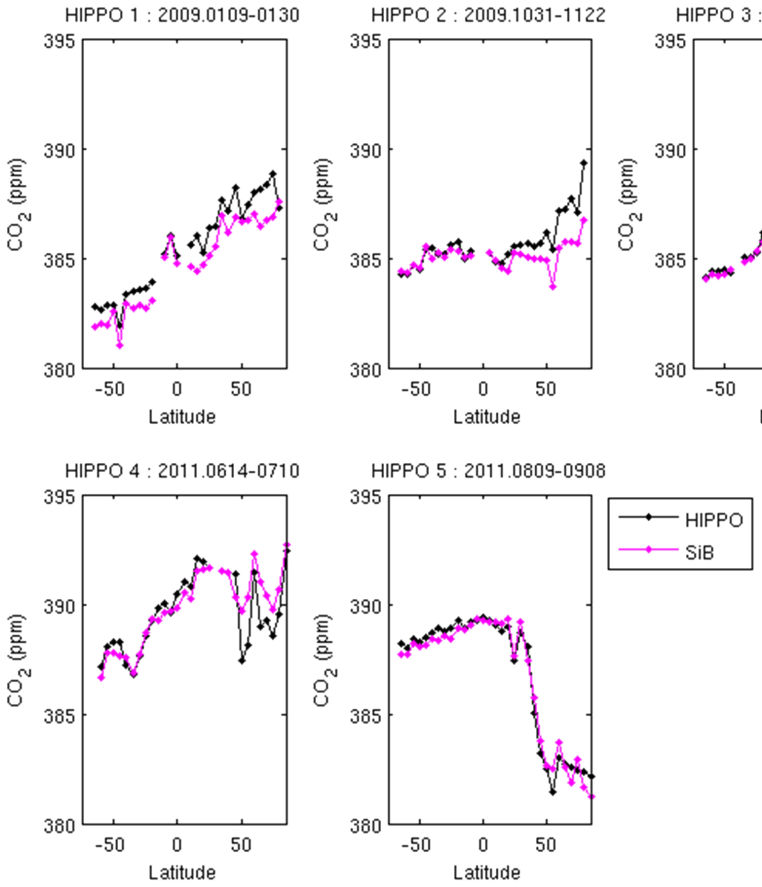

Figure 7. Comparison of HIPPO CO_2 measurements (black) and model simulations with SiB land fluxes (magenta).

ACPD
15, 26025–26065, 2015

Towards understanding the variability in biospheric CO_2 fluxes

Y. Wang et al.